Basal PPARα inhibits bile acid metabolism adaptation in chronic cholestatic model induced by α-naphthylisothiocyanate

Huiying Hua[a,1], Manyun Dai[a,b,c,1], Yishuang Luo[a], Hante Lin[a], Gangming Xu[a], Xiaowei Hu[a], Liping Xu[a], Haoyue Zhang[a], Zhiyuan Tang[a], Liming Chang[a], Aiming Liu[a,*], Julin Yang[d,*]

[a] Medical School of Ningbo University, Ningbo 315211, China
[b] State Key Laboratory of Phytochemistry and Plant Resources in West China, Kunming Institute of Botany, Chinese Academy of Sciences, Kunming, 650201, China
[c] University of Chinese Academy of Sciences, Beijing 100049, China
[d] Ningbo College of Health Sciences, Ningbo 315100, China

ARTICLE INFO

ABSTRACT

Cholestasis is one of the most challenging diseases to be treated in current hepatology. However little is known about the adaptation difference and the underlying mechanism between acute and chronic cholestasis. In this study, wild-type and *Pparα*-null mice were orally administered diet containing 0.05% ANIT to induce chronic cholestasis. Biochemistry, histopathology and serum metabolome analysis exhibited the similar toxic phenotype between wild-type and *Pparα*-null mice. Bile acid metabolism was strongly adapted in *Pparα*-null mice but not in wild-type mice. The *Shp* and *Fxr* mRNA was found to be doubled in cholestatic *Pparα*-null mice compared with the control group. Western blot confirmed the up-regulated expression of FXR in *Pparα*-null mice treated with ANIT. Inflammation was found to be stronger in *Pparα*-null mice than those in wild-type mice in chronic cholestasis. These data chain indicated that bile acid metabolism and inflammation signaling were different between wild-type and *Pparα*-null mice developing chronic cholestasis, although their toxic phenotypes could not be discriminated. So basal PPARα cross-talked with FXR and inhibited bile acid metabolism adaptation in chronic cholestasis.

1. Introduction

Cholestasis is a disease caused by impaired balance among bile acid synthesis, conjugation, uptake and excretion (Ofliver, 2009). Primary sclerosing cholangitis (PSC) and primary biliary cirrhosis (PBC) are the most common cholestatic liver diseases in the clinic (Nguyen et al., 2014). The prevalence of PSC was as high as 162 per million in US (Molodecky et al., 2011). For PBC, the prevalence was reported to be 492 and 208 cases per million people in southern China and South Asian countries respectively (Sood et al., 2004; Liu et al., 2010). Clinically, cholestasis caused secondary organ dysfunctions in gastroenterology (Gubergrits and Lukashevich, 2014). Liver transplantation became necessary for more than 50% of PSC patients 10–15 years after

symptom development (Kubitz et al., 2015; Stephanie et al., 2018). Thus, cholestasis is still one of the most challenging diseases to be treated in current hepatology.

Cholestatic models used in basic studies were usually induced by alpha-naphthylisothiocyanate (ANIT), lithocholic acid (LCA) and 3, 5-diethoxycarbonyl-1, 4-dihydrocollidine (DDC) (Marhenke et al., 2014; Wang et al., 2014; Zhang et al., 2015). The pathological and physiological reactions of ANIT-induced cholestasis were considered the most similar to intrahepatic cholestasis in human (Tjandra et al., 2000). So this cholestatic model was used very often in toxicological and pharmacological researches (Ding et al., 2012; Wang et al., 2014; Chen et al., 2016). In 129/Sv mice treated with single dose of ANIT (75 mg kg^{-1}), the liver injury was most obvious 48 h later (Dai et al.,

Fig. 1. Biochemical analysis of liver tissues after ANIT treatment. (A) TBA in wild-type and *Ppara*-null mice respectively. (B) ALP in the wild-type and *Ppara*-null mice. (C) TBIL in wild-type and *Ppara*-null mice. (D) DBIL in wild-type and *Ppara*-null mice. (E) ALT in wild-type and *Ppara*-null mice respectively. (F) AST in the wild-type and *Ppara*-null mice. The data were expressed as mean ± SD (n = 5, *: compared with WT-C/KO-C; *P* < 0.05).

2018). In rats treated with single dose of ANIT (50 mg kg^{-1}), the liver injury and bile duct proliferation were observed after 3 days (Chen et al., 2015). However, cholestatic liver diseases in the clinic were mostly chronic (Ferreira et al., 2003). It is necessary to investigate more about the pathophysiology of chronic cholestasis.

When 75 mg/kg^{-1} ANIT (ig) was administered to Sprague-Dawley rats, the *Cyp7a1, Cyp8b1, Cyp27a1* and *Oatp2* were down-regulated, while the *Ostb, Mdr1* and *Mdr2* were up-regulated (Yuan et al., 2017). In Wistar rats treated with a dose of ANIT 50 mg kg^{-1}, the OATP1 was down-regulated, but MRP2 and BSEP were up-regulated (Zhang et al., 2016). In C57BL/6 mice treated with a single dose of ANIT (75 mg/kg^{-1}, ig), the *Bsep, Mdr2 and Mrp3* mRNAs were increased. Similarly the *Nctp* and *Oatp1* mRNAs were decreased (Tanaka et al., 2009). These responses of bile acid synthesis and transport in the acute models result in decrease of bile acid load and toxicity risk in hepatocytes, which were considered as adaptation (Jang et al., 2012; Firrincieli et al., 2013). However, in a rat model dosed ANIT (80 mg/kg^{-1}, once a week) for 8 weeks, the *Mrp3* and *Mrp4* expression only increased 0.8-fold (Cai et al., 2014). In a mouse model treated with DDC for 5 months, the *Mdr2* mRNA only increased 1.8-fold compared with the control (Marhenke et al., 2014). Thus bile acid metabolism exhibited very milder modifications in chronic cholestatic models than those in acute models. But it is not well known why this difference occurs and what its contribution to toxicity in cholestasis is.

Peroxisome proliferator-activated receptor alpha (PPARα) played an important role in bile acid homeostasis (Zhou et al., 2014; Luo et al.,

2017). In mice treated with WY-14,643 for 1 week, an increase of gallbladder cholic acid was observed, which did not occur in the *Ppara*-null mice (Hunt et al., 2000). In another study where mice were dosed a gemfibrozil-containing diet for 14 days, PPARα mediates hepatotoxicity in part by disrupting bile acid homeostasis in wild-type mice (Liu et al., 2014a). Similarly, PPARα agonist ciprofibrate reduced CYP7A1 and CYP27A1 activity and mRNA levels in wild-type mice, not *Ppara*-null mice (Post et al., 2001). In contrast, when mice were treated with a cholic acid diet, neither metabolic disorder nor the regulation of bile acid synthesis was noted in wild-type mice (Li et al., 2012). In our previous study, the basal PPARa also played a protective role in acute cholestatic model (Dai et al., 2017). So PPARα, activated and basal level, are protective or disruptive for bile acid homeostasis, suggesting its involvement in disease development and potential for clinical therapeutics. However, it was still uncertain what the role of PPARα in chronic cholestatic models was.

In this study, wild-type and *Ppara*-null mice were fed a diet containing ANIT (0.05%) to induced chronic cholestasis and liver injury. The different adaptation of bile acid metabolism and inflammatory response between wild-type and *Ppara*-null mice were revealed, suggesting the potential cross-talk between PPARα and Farnesoid X receptor (FXR).
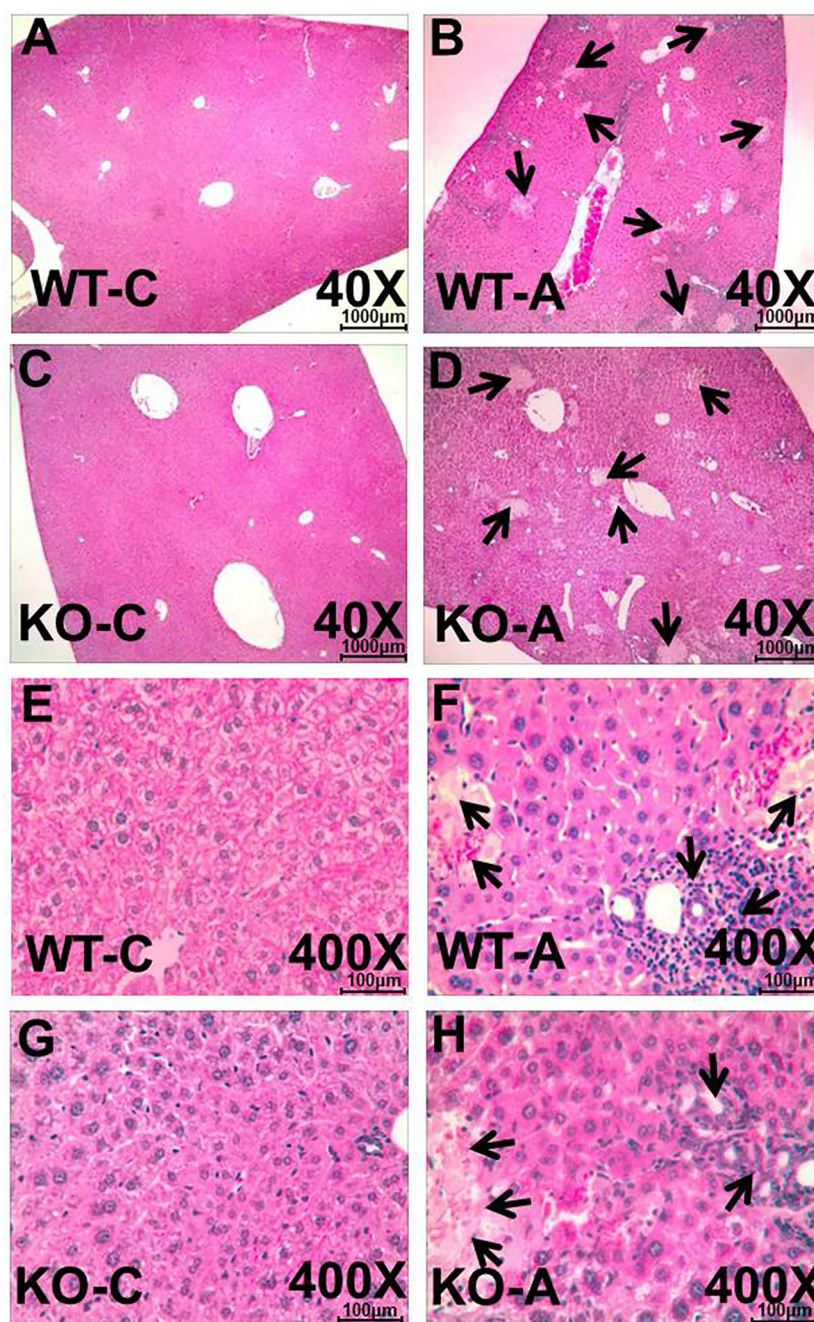
Fig. 2. Hepatotoxicity analysis of liver tissues after ANIT treatment. (A) HE staining of liver tissues in the WT-C group (40X). (B) HE staining of liver tissues in the WT-A group (40X). (C) HE staining of liver tissues in the KO-C group (40X). (D) HE staining of liver tissues in the KO-A group (40X). (E) HE staining of liver tissues in the WT-C group (400X). (F) HE staining of liver tissues in the WT-A group (400X). (G) HE staining of liver tissues in the KO-C group (400X). (H) HE staining of liver tissues in the KO-A group (400X). Arrows: exhibited a loss of cellular boundaries, degenerative changes and marked necrosis.

2. Materials

2.1. Chemicals and reagents

Assay kits for the liver injury markers alkaline phosphatase (ALP), aspartate aminotransferase (AST), alanine aminotransferase (ALT) and cholestasis markers total bile acid (TBA) were purchased from Ruiyuan Biotechnology (Ningbo, China). ANIT, tauroursodeoxycholic acid (TUDCA), taurodeoxycholic acid (TDCA), tauro-α-muricholic acid (TαMCA), tauro-ω-muricholic acid (TωMCA), taurocholic acid (TCA) and taurochenodeoxycholic acid (TCDCA) were purchased from Sigma-Aldrich (St Louis, MO). Antibodies against Cholesterol 7α hydroxylase (Cyp7A1), sterol 12α-hydroxylase (Cyp8B1) and GAPDH were acquired from Abcam (MA, USA). TRIzol solution was purchased from Invitrogen (Dalian, China). BCA protein assay kit was from Beyotime Biotech Co. Ltd (Nantong, China) and PMSF was bought from Solarbio (Shanghai, China). The reverse transcription kit and LightCycle 480 SYBR Green I Master Mix were purchased from Roche Diagnostics (Mannheim, Germany). Ultrapure water was freshly prepared using a Milli-Q50 SP Water System (MA, USA). All the other chemicals were of the highest grade available from commercial sources.
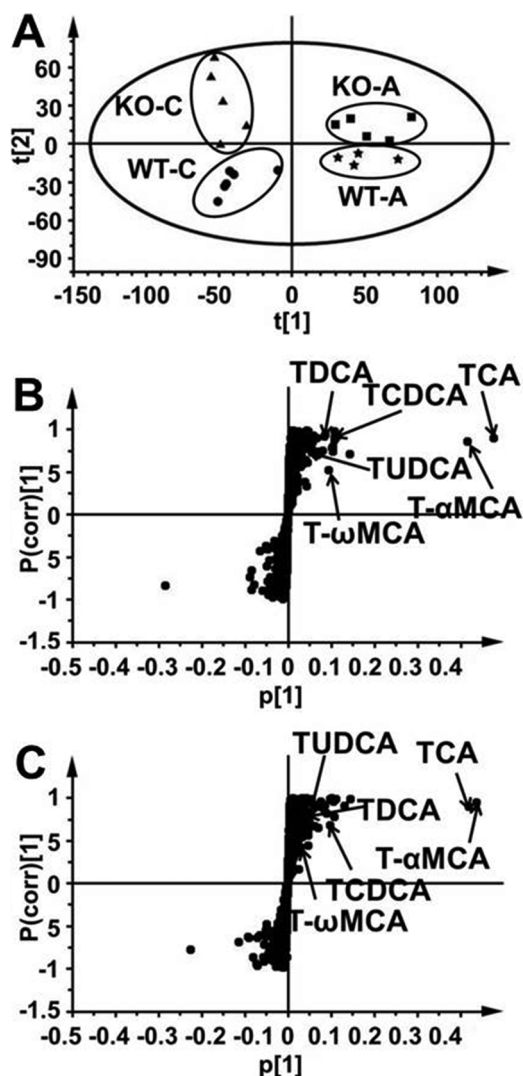
Fig. 3. Multivariate data analysis of serum metabolome in mice dosed ANIT. (A) Score plot of serum metabolite in ANIT treated wild-type (WT) and *Ppara-null* (KO) mice versus their control groups by PCA. (B) S scatter plot of OPLS-DA recognized serum metabolome in ANIT-treated WT mice versus WT-C mice, in which contribution of identified bile acids were indicated. (C) S scatter plot of OPLS-DA recognized serum metabolome in ANIT-treated KO mice versus KO-C mice, in which contribution of identified bile acids were indicated. The t[1]and t[2] represent principal components 1 and 2, respectively. The p(corr)[1] represents the interclass difference, and p[1] represents the relative abundance of the ions (PCA, principal component analysis; OPLS-DA, orthogonal projection to latent tructures discriminant analysis).

## 2.2. Animals and treatments

The *Ppara*-null mice were gifted by Dr. Frank J. Gonzalez at Laboratory of Metabolism, National Cancer Institute, NIH. They were hybrid with local 129/Sv wild-type mice for several generations, and then genotype was performed to choose out those homozygote. This made sure the *Ppara*-null and wild-type mice used in this study shared the same genetic background. Animal procedures followed the Institute of Laboratory Animal Resource guidelines, and the protocols were approved by the Animal Care and Use Committee of Ningbo University. Before the experiments, 24 to 28 g male wild-type and *Ppara*-null mice were housed at the Medical School of Ningbo University Animal Center for 7 days of acclimation at 23 ± 1 °C, with a humidity of 60 − 70%. The mice were maintained under a standard 12 h light/12 h dark cycle with free access to water and a commercial diet (20708660330000)
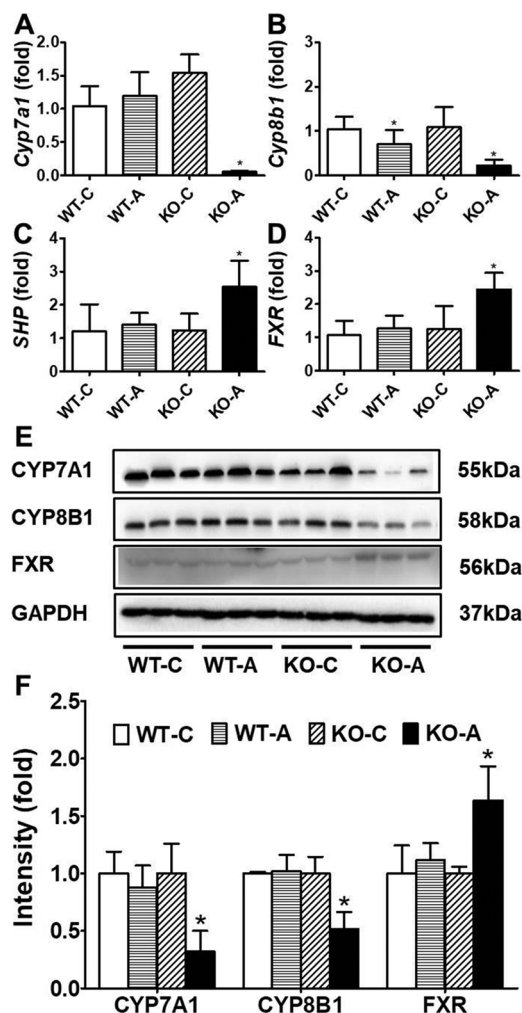
Fig. 4. Different expression of FXR pathway in two mouse lines. (A) *Cyp7a1* mRNA levels in the wild-type and *Ppara*-null mice. (B) *Cyp8b1* mRNA in wild-type and *Ppara*-null mice. (C) *SHP* mRNA levels in the wild-type and *Ppara*-null mice. (D) *FXR* mRNA levels in the wild-type and *Ppara*-null mice respectively. The mRNA levels were measured by Q-PCR and normalized by *18SrRNA*. (E) Western-blot analysis of differential CYP7A1, CYP8B1 and FXR signaling mediated by PPARα. (F) The Western-blot intensity of CYP7A1, CYP8B1 and FXR in the wild-type and *Ppara*-null mice respectively. Data were from liver samples collected 48 h after ANIT treatment and 2/5 of the liver tissues were randomly selected for western-blot analysis. The mRNAs levels in the vehicle-treated control mice were set as 1 and the results expressed as mean ± SD (n = 5, *: compared with WT-C/KO-C; *$P < 0.05$).

purchased from Zhejiang Institute of Laboratory Animal Resource.

Two mouse lines were randomly assigned into four groups: wild-type/vehicle (WT-C), wild-type/ANIT (WT-A), *Ppara*-null/vehicle (KO-C), and *Ppara*-null/ANIT (KO-A). The positive groups were treated with commercial diet contained ANIT (0.05%) (The daily dose was estimated as 60 mg/kg^{-1}). Tail bleeding was performed to collect blood for biochemical analysis. When the serum TBA and liver injury biomarkers became stable, the model was considered established. It took 15 days for the wild-type mice and 8 days for the *Ppara*-null mice respectively to induce this chronic model. All mice were weighed and killed using carbon dioxide asphyxiation. Blood and liver tissues were collected for mechanism investigation. A section of freshly isolated liver tissues was excised and immediately fixed in 10% neutral buffered formalin after a brief wash using phosphate-buffered saline (PBS). The remaining tissues were flash-frozen and stored at − 80 °C pending analysis.
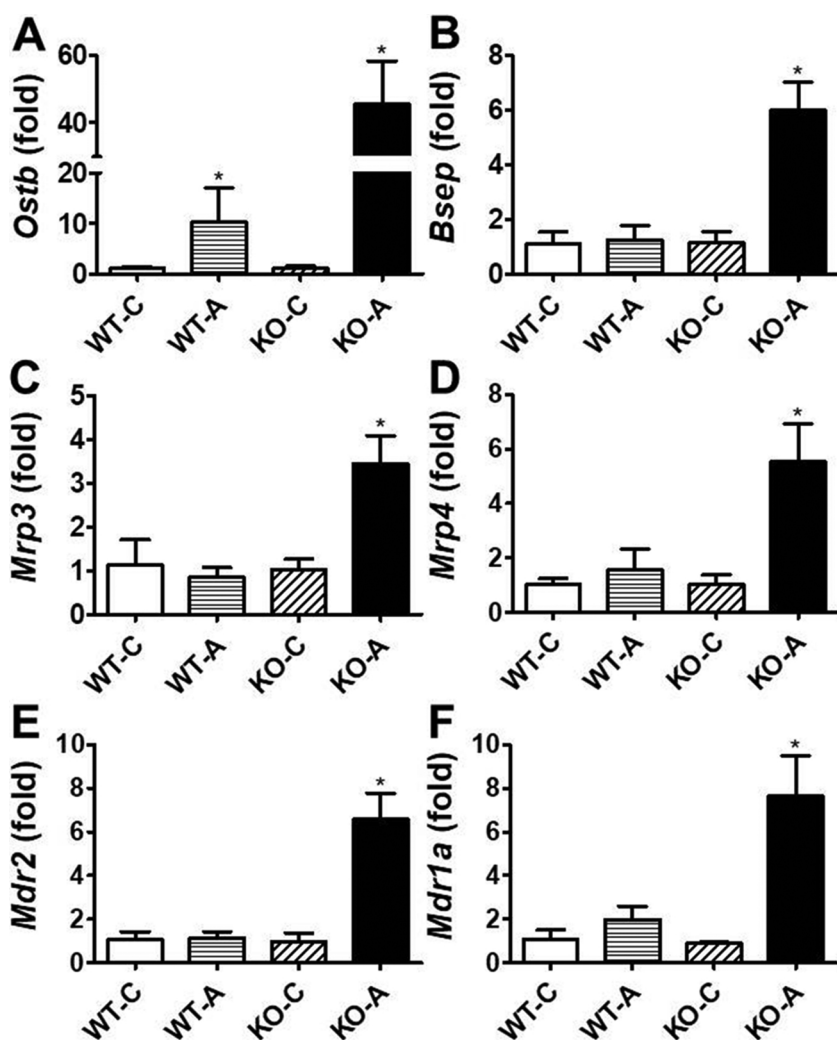
Fig. 5. Different regulated expression of genes involved in bile acid canalicular efflux transporters and basolateral efflux transporters transport. (A) *Ostb* mRNA levels in the wild-type and *Ppara*-null mice respectively. (B) *Bsep* mRNA levels in the wild-type and *Ppara*-null mice respectively. (C) *Mrp3* mRNA levels in the wild-type and *Ppara*-null mice respectively. (D) *Mrp4* mRNA levels in the wild-type and *Ppara*-null mice respectively. (E) *Mdr2* mRNA levels in the wild-type and *Ppara*-null mice respectively. (F) *Mdr1a* mRNA levels in the wild-type and *Ppara*-null mice respectively. The mRNAs levels in the vehicle-treated control mice were set as 1 and the results expressed as mean ± SD (n = 5, *: compared with WT-C/KO-C; *P* < 0.05).

2.3. Biochemical analysis

The liver tissues from different groups were accurately quantified and then homogenized by MagNALyser (Roche, USA). TBA, ALP, TBIL, DBIL, ALT, and AST in serum were assayed by the Multiskan GO (Thermo, USA). The measurements were carried out following protocols in the kits.

2.4. Histopathological assessment

Formalin fixed liver tissues were dehydrated in alcohol and xylene following the standard procedures and embedded by paraffin for preparation of four-micrometer sections. After staining with hematoxylin and eosin, the liver sections were examined under a microscope (Olympus BX41). 10 serial sections per preparation were imaged, and all images were analyzed blindly.

### 2.5. Quantitative polymerase chain reaction (Q-PCR) analysis

The total RNA extraction, the reverse transcription of cDNA, the amplification program was the same as published procedures (Tan et al., 2016). The primer sequences extracted from a public database (http://mouseprimerdepot.nci.nih.gov) were listed in Supplementary table 1. A 5 μL PCR system was designed for the 384 plate that included 1 μL of total cDNA, 2.5 μL of LightCycle 480 SYBR Green I Master Mix, 0.2 μL of forward and reverse primer, and 1.1 μL of nuclease-free water.

2.6. Western blot analysis

Liver tissues were homogenized using RIPA buffer (1:10, g/v) containing 1% PMSF. Tissue debris was removed by centrifugation at 10,000 g and 4 °C for 15 min. The total protein was quantified using a BCA protein assay kit. An equivalent volume of 5 X SDS-PAGE sample loading buffer was added to the tubes that were then boiled for 5 min. The samples were loaded and separated on 10% SDS-polyacrylamide gels and then transblotted onto PVDF membranes. The membranes were blocked with 5% fat-free milk at 37 °C for at least 2 h followed by incubation overnight with primary antibodies against the indicated antigens. After secondary antibody incubation for 1 h, the blotted membranes were exposed to ECL substrates and the signals were detected by Tanon 4200SF (Shanghai, China).

2.7. Analysis of serum metabolome

In the metabolomic analysis, the serum samples were processed and infused into the Ultra Performance Liquid Chromatography-Time of Flight Mass (UPLC-TOFMS) detection system following previously published procedures (Dai et al., 2018). After being processed by Marker Lynx, a data matrix of peak areas organized by retention time and *m/z* was generated and then exported into SIMCA 13.0.3 (Umetrics, Kinnelon, NJ) for pareto transformation. Then unsupervised principal component analysis (PCA) was used to produce score plots. Orthogonal projection to latent structures discriminant analysis (OPLS-DA) was exploited to produce the loading S-plot of ANIT-treated mice versus the
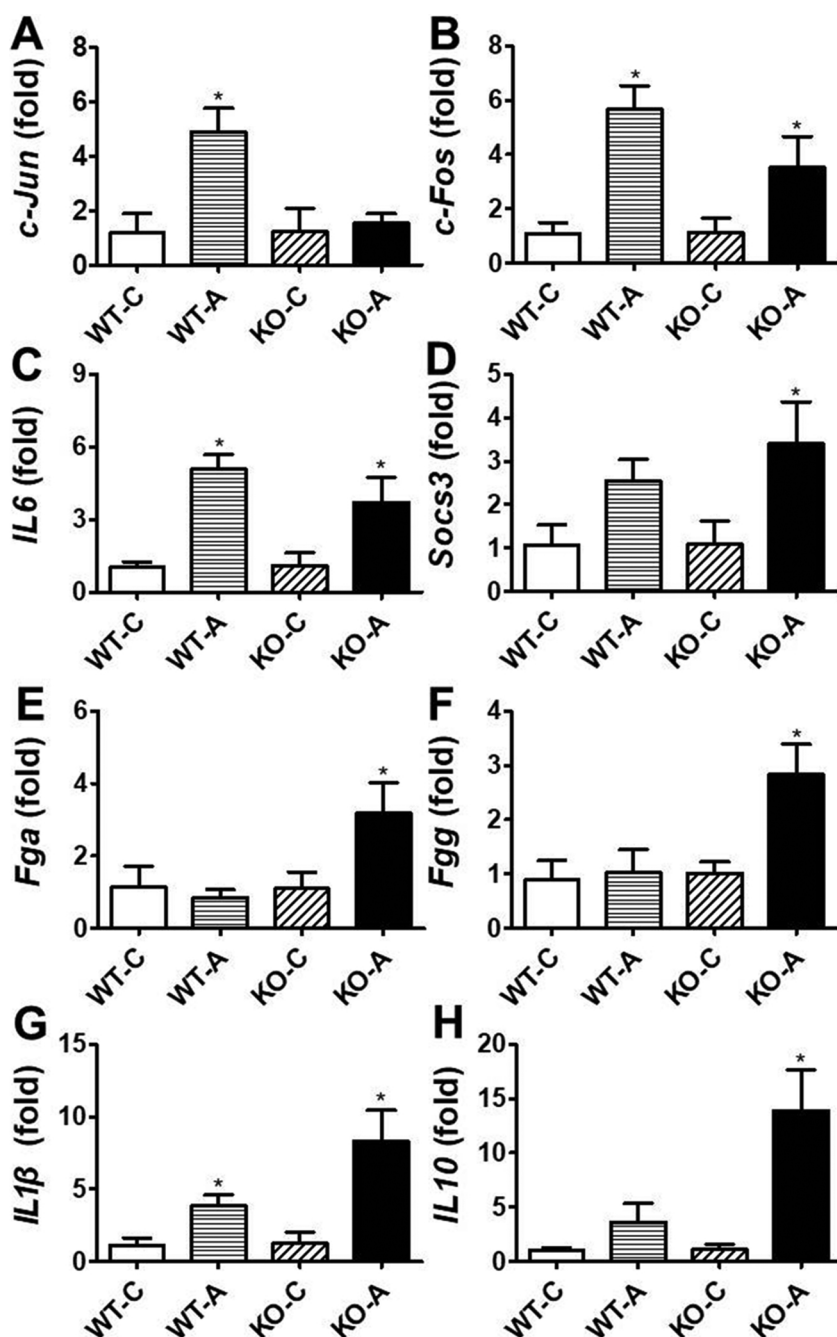
Fig. 6. Differential expression of pro-inflammatory factors associated with JNK and STAT3 signaling. (A, B) *c-Jun* and *c-Fos* mRNA levels in the wild-type and *Ppara*-null mice respectively. (C) *Il6* mRNA levels in the wild-type and *Ppara*-null mice. (D, E and F) *Socs3, Fga* and *Fgg* mRNA levels in the wild-type and *Ppara*-null mice respectively. (G) *Ilβ* mRNA levels in the wild-type and *Ppara*-null mice respectively. (H) *Il10* mRNA levels in the wild-type and *Ppara*-null mice. The mRNA levels were measured by Q-PCR and normalized by *18SrRNA* mRNA levels in the vehicle-treated control mice were set as 1 and the results expressed as mean ± SD(n = 5, *: compared with WT-C/KO-C; *$P < 0.05$).
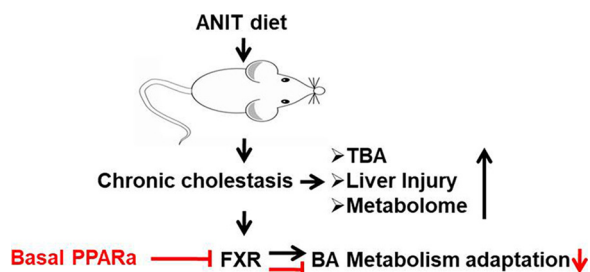
Fig. 7. Proposed action mode of basal PPARa inhibiting bile acid metabolism adaptation in chronic cholestatic model induced by ANIT. Wild-type and *Ppara*-null mice were orally administered commercial diet containing 0.05% ANIT to induce chronic cholestasis. The FXR pathway was found to be activated in *Ppara*-null mice but not in wild-type mice. So basal PPARα cross-talked with FXR and inhibited bile acid metabolism adaptation in chronic cholestasis.

control mice, in which the BAs contributing to the pattern recognition were exhibited.

To quantitatively show the similarity of the above metabolome shift, the contributing items were compared with authentic BA compounds. Some of them were identified as TUDCA, TDCA, TCDCA, TCA and T-α/ωMCA by comparison of the tandem mass spectrometry (MS/MS) spectra. The relative abundance of these BAs in the serum was normalized by comparing their peak areas with those of internal standard. Fold changes versus the wild-type control group were used to express their systemic abundance in the ANIT-treated mice.

2.8. Statistical analysis

All the data were expressed as the mean ± SD. SPSS 23 (IBM) for Windows was used for the data analysis. The two-sample *t*-test was used to compare the diff ;erences between the ANIT treatment and control

groups respectively, and no comparison between two mouse lines was made. Significant diff ;erence was decided when $P < 0.05$ and was marked with asterisks in the graphs accordingly.

3. Results

3.1. Toxic phenotypes between wild-type and Pparα-null mice were similar

The serum TBA was increased by 19-fold and 24-fold in wild-type and *Pparα*-null mice treated with ANIT compared with control mice (Fig. 1A). The ALP in this model exhibited no change after treatment with ANIT (Fig. 1B). The TBIL and DBIL were both sharply increased in two mouse lines after treatment with ANIT (P values were below 0.05, Fig. 1C and D). The ALT and AST were increased by 9-fold and 12-fold respectively in WT-A mice. In KO-A mice, they were increased by 20-fold and 5-fold compared with KO-C group (P values were below 0.05, Fig. 1E and F).

Pathological analysis of the hepatic tissues in both WT-C and KO-C groups exhibited normal histology. In WT-A and KO-A groups, a loss of cellular boundaries, degenerative changes and marked necrosis were observed (Fig. 2A to H). The histopathological observations were not different between WT-A and KO-A mice.

3.2. Serum metabolome comparison between wild-type and Pparα-null mice

In an unsupervised PCA analysis of the data sets from 4 groups of mice, the samples in WT-A and KO-A mice clustered together respectively but closed to each other. They both moved rightward in parallel compared with the control mice. This change indicated the metabolome difference in two mouse lines was weakened by ANIT and they were modified in a quite similar manner (Fig. 3A).

In S-plots produced by OPLS-DA analysis between ANIT-treated groups vs control groups of two mouse lines (Fig. 3B, C), 6 contributing ions were identified as TCA, TUDCA, TCDCA, TDCA, T-αMCA and T-ωMCA by comparison with authentic standards. After normalization and relative quantification of peak areas of the above components, their relative abundance in serum was found to be quite similar between two mouse lines (Supplementary Fig. 1).

3.3. PPARα inhibited bile acid metabolism adaptation via cross-talk with FXR

The *Cyp7a1* and *Cyp8b1* mRNAs level in the WT-A groups was not different from those in the WT-C groups. But the *Cyp7a1* and *Cyp8b1* mRNAs level in the *Pparα*-null mice was decreased by 96.47% and 79.28% respectively (P values were below 0.05, Fig. 4A and B). *Shp* mRNA was increased by 1-fold (P values were below 0.05) in the KO-A group, but no increase in the WT-A group was observed (Fig. 4C). For FXR, its mRNA level in WT-A was similar as the WT-C group, but in *Pparα*-null mice, its mRNA level was also doubled compared with KO-C group (Fig. 4D).

In western blot analysis, the CYP7A1 and CYP8B1 were inhibited in the KO-A group, but no inhibition was observed in wild-type mice (Fig. 4E and F). The protein level of FXR was obviously up-regulated in KO-A group, which did not occur in WT-A group. Combining the above Q-PCR analysis and WB results, the bile acid metabolism adaptation was strongly adapted in *Pparα*-null mice and it was supposed to be mediated by FXR pathway. The expression of PPARα target genes (*Ehhadh* and *Acox1*) were not increased in two mouse lines (data not shown), but the adaptation was almost totally inhibited in wild-type mice. So the bile acid metabolism was inhibition in wild-type mice was mediated by cross-talk between basal PPARα and FXR signaling.

The *Ostb* mRNA in WT-A group was increased by 8-fold ($P < 0.05$). But in the KO-A group, the level of *Ostb* mRNA was increased by 41-fold compared with the control mice ($P < 0.05$) (Fig. 5A). *Bsep, Mrp3, Mrp4, Mdr2* and *Mdr1a* were increased by 4-fold, 2-fold, 4-fold, 5-fold

and 7-fold respectively in KO-A group (P values were below 0.05). But in wild-type mice, their increases were not observed (Fig. 5B, C, D. E and F). However, there was an exception, the *oatp1* mRNA decreased in two mouse lines and showed no difference between WT-A and KO-A group (85.32% and 92.53%, P values were below 0.05) (Supplementary Fig. 2). Taken together, the *Ostb, Besp, Mrp3, Mrp4, Mdr2* and *Mdr1a* were adaptively modified in *Pparα*-null mice, not the wild-type mice, indicating their adaptation was also inhibited by PPARα.

3.4. Basal PPARα inhibited inflammation in chronic cholestasis

c-Jun and *c-Fos* mRNAs were increased by 3-fold and 4-fold in the WT-A group compared with WT-C group (P values were below 0.05). In *Pparα*-null mice, *c-Jun* and *c-Fos* were not changed by ANIT (Fig. 6A and B). *Il6* was increased by 5-fold and 3-fold in wild-type mice and *Pparα*-null mice respectively. It was obviously increased compared with control group (P values were below 0.05), but there was no difference between two mouse lines (Fig. 6C). *Socs3, Fga* and *Fgg* mRNAs were increased obviously in the KO-A group (2.12-fold, 1.9-fold and 1.8-fold, P values were below 0.05), and no change in the WT-A group (Fig. 6D, E and F). These data indicated the STAT3 pathway was activated in *Pparα*-null mice, not the wild-type mice. *Il1β* and *Il10* mRNAs were increased by 6-fold and 12-fold in the KO-A group compared with KO-C group (P values were below 0.05), but the difference of *Il1β* and *Il10* between WT-C and WT-A were very slight (Fig. 6G and H).

4. Discussion

In this study, chronic cholestatic model was successfully induced by feeding the wild-type mice and *Pparα*-null mice ANIT (0.05%)-containing diet. Serum TBA, ALT and AST increased similarly in two mouse lines treated with ANIT. However, the ALP in this model was not modified by ANIT treatment in two mouse lines. In previous studies (Dai et al., 2017; Luo et al., 2017), the ALP was sharply increased in acute cholestasis models. This difference was supposed to relate with adaptation of bile duct injury in chronic cholestasis. In the results of pathological analysis, no obvious difference was observed. Bile acid component TCA, TUDCA, TCDCA, TDCA, T-αMCA and T-ωMCA were also similarly abundant between wild-type mice and *Pparα*-null mice. So, the toxic phenotypes induced by ANIT in chronic cholestasis were the same between two mouse lines (Fig. 7).

In acute cholestatic model induced by perfluorodecanoic acid, the *Cyp8b1* and *Oatp1* mRNAs were decreased by 71%, 53% and 99%, 50% in wild-type mice and *Pparα*-null mice respectively (Luo et al., 2017). In wild-type mice and *Pparα*-null mice treated with single dose of ANIT ($75 \, \text{mg/kg}^{-1}$, ig), the *Cyp7a1, Cyp8b1, Oatp1* and *Oatp2* were decreased by 96.74%, 94.22%, 53.83% and 56.25% in wild-type mice at 48 h. In *Pparα*-null mice, these genes were decreased by 99.87%, 92.85%, 82.37% and 85.52%. The level of *Ostb* increased by 204-fold and 225-fold respectively, the *Mrp4* increased by 6.2-fold and 5.3-fold respectively in wild-type mice and *Pparα*-null mice. The two mouse lines exhibited the same change (Dai et al., 2018). In this study, *Cyp7a1* and *Cyp8b1* were decreased by 96.47% and 79.28% respectively in KO-A mice, the *Besp, Mrp3, Mrp4, Mdr2* and *Mdr1a* genes were all increased by 4.27-fold, 2.37-fold, 4.31-fold, 5.69-fold and 7.62-fold respectively in KO-A group. But in wild-type mice, all these genes were exhibited no difference between control and ANIT-treated mice. These data indicated the strong potential of PPARa to inhibit adaptation in chronic cholestasis.

FXR is a master regulator maintaining the homeostasis of bile acids (Sinal et al., 2000). FXR induced small heterodimer partner (SHP) and FGF15 in the liver to inhibit the expression of CYP7A1, OSTB, MDR1 and MDR2 involved in bile acid synthesis and transport (Arrese and Karpen, 2001; Inagaki et al., 2005; Modica et al., 2012). In this study, *Fxr* mRNA was doubled in *Pparα*-null mice by ANIT, and the WB result confirmed this up-regulation. *Shp* mRNA was found a 1.06-fold

increase. However, these modifications did not occur in wild-type mice. The expression of *Cyp7a1*, *Cyp8b1* and transport genes (*Besp, Mrp3, Mrp4, Mdr2* and *Mdr1a*) were also up-regulated in *Ppara*-null mice, not in wild-type mice, which were confirmed by WB. These differences were all supposed to be regulated by the cross-talk between the basal PPARa and FXR signaling.

Liver injury was associated with inflammation pathways including JNK, NF-κB and STAT3 in acute models (Li et al., 2006; Liu et al., 2014b; Ghonem et al., 2015). In mice treated with ANIT, the activation of PPARα by Wy-14, 643 decreased the NF-κB/IL-6/STAT3 signaling, and reduced liver injury (Fang et al., 2017). In acute cholestatic model induced by ANIT (75 mg/kg, ig), basal PPARa inhibited NF-κB/STAT3 signaling leading to decreased toxic response (Dai et al., 2018). In this study, the inflammation was also obviously increased in KO-A mice and no obvious change was observed in WT-A mice. The expression of STAT3 target genes *Socs3, Fga* and *Fgg* mRNAs was increased in the KO-A mice but not in the wild-type mice. These data supported that basal PPARa played an anti-inflammation role in chronic cholestasis, agreeing with that in acute cholestatic models.

Conclusively, the toxic phenotypes were similar between wild-type and *Ppara*-null mice in chronic cholestatic model. Cross-talk between basal PPARα and FXR inhibited bile acid metabolism adaptation (Fig. 7). However, underlying the similar toxic phenotypes, basal PPARα played a more important role in anti-inflammation than regulating adaptation to decrease toxicity.

Financial support

Conflict of interest

The authors who have taken part in this study declared that they do not have anything to disclose regarding funding or conflict of interest with respect to this manuscript.

Authorship contributions

HH participated in research design, conducted experiments, performed data analysis and wrote the writing of the manuscript. MD participated in research design, conducted experiments and contributed new reagents or analytic tools. YL participated in performing experiment in revision of this manuscript. HT, GX, XH, LX and HZ conducted experiments, performed data analysis and contributed new reagents or analytic tools. ZT and LC conducted experiments and data analysis. AL and JY designed this project, performed data analysis and wrote this manuscript.

Appendix A. Supplementary data

Supplementary data associated with this article can be found, in the online version, at https://doi.org/10.1016/j.toxlet.2018.10.015.

References

Arrese, M., Karpen, S.J., 2001. New horizons in the regulation of bile acid and lipid homeostasis: critical role of the nuclear receptor FXR as an intracellular bile acid sensor. Gut 49, 465–466.

Cai, S.Y., Mennone, A., Soroka, C.J., Boyer, J.L., 2014. All-trans-retinoic acid improves cholestasis in alpha-naphthylisothiocyanate-treated rats and Mdr2-/- mice. J. Pharmacol. Exp. Ther. 349, 94–98.

Chen, H., Huang, X., Min, J., Li, W., Zhang, R., Zhao, W., Liu, C., Yi, L., Mi, S., Wang, N.,

Wang, Q., Zhu, C., 2016. Genip) posidic acid protected against ANIT-induced hepatotoxity and acute intrahepatic cholestasis, due to Fxr-mediated regulation of Bsep and Mrp2. J. Ethnopharmacol. 179, 197–207.

Chen, Z., Ma, X., Zhu, Y., Zhao, Y., Wang, J., Li, R., Chen, C., Wei, S., Jiao, W., Zhang, Y., Li, J., Wang, L., Wang, R., Liu, H., Shen, H., Xiao, X., 2015. Paeoniflorin ameliorates ANIT-induced cholestasis by activating Nrf2 through an PI3K/Akt-dependent pathway in rats. Phytother. Res. 29, 1768–1775.

Dai, M., Hua, H., Lin, H., Xu, G., Hu, X., Li, F., Gonzalez, F.J., Liu, A., 2018. Targeted metabolomics reveals a protective role for basal PPARalpha in cholestasis induced by alpha-naphthylisothiocyanate. J. Proteome Res. 17, 1500–1508.

Dai, M., Yang, J., Xie, M., Lin, J., Luo, M., Hua, H., Xu, G., Lin, H., Song, D., Cheng, Y., Guo, B., Zhao, J., Gonzalez, F.J., Liu, A., 2017. Inhibition of JNK signalling mediates PPARalpha-dependent protection against intrahepatic cholestasis by fenofibrate. Br. J. Pharmacol. 174, 3000–3017.

Ding, L.L., Zhang, B.F., Dou, W., Yang, L., Zhan, C.S., Wang, Z.T., 2012. Protective effect of Danning tablet on acute livery injury with cholestasis induced by alpha-naphthylisothiocyanate in rats. J. Ethnopharmacol. 140, 222–229.

Fang, Z.Z., Tanaka, N., Lu, D., Jiang, C.T., Zhang, W.H., Zhang, C., Du, Z., Fu, Z.W., Gao, P., Cao, Y.F., Sun, H.Z., Zhu, Z.T., Cai, Y., Krausz, K.W., Yao, Z., Gonzalez, F.J., 2017. Role of the lipid-regulated NF-kappaB/IL-6/STAT3 axis in alpha-naphthyl isothiocyanate-induced liver injury. Arch. Toxicol. 91, 2235–2244.

Ferreira, F.M., Oliveira, P.J., Rolo, A.P., Santos, M.S., Moreno, A.J., da Cunha, M.F., Seica, R., Palmeira, C.M., 2003. Cholestasis induced by chronic treatment with alpha-naphthyl-isothiocyanate (ANIT) affects rat renal mitochondrial bioenergetics. Arch. Toxicol. 77, 194–200.

Firrincieli, D., Zuniga, S., Rey, C., Wendum, D., Lasnier, E., Rainteau, D., Braescu, T., Falguieres, T., Boissan, M., Cadoret, A., Housset, C., Chignard, N., 2013. Vitamin D nuclear receptor deficiency promotes cholestatic liver injury by disruption of biliary epithelial cell junctions in mice. Hepatology 58, 1401–1412.

Ghonem, N.S., Assis, D.N., Boyer, J.L., 2015. Fibrates and cholestasis. Hepatology 62, 635–643.

Gubergrits, N.B., Lukashevich, G.M., 2014. Cholestasis and pancreatic insufficiency: how to start treatment? Exp. Clin. Gastroenterol. 84.

Hunt, M.C., Yang, Y.Z., Eggertsen, G., Carneheim, C.M., Gafvels, M., Einarsson, C., Alexson, S.E., 2000. The peroxisome proliferator-activated receptor alpha (PPARalpha) regulates bile acid biosynthesis. J. Biol. Chem. 275, 28947–28953.

Inagaki, T., Choi, M., Moschetta, A., Peng, L., Cummins, C.L., McDonald, J.G., Luo, G., Jones, S.A., Goodwin, B., Richardson, J.A., Gerard, R.D., Repa, J.J., Mangelsdorf, D.J., Kliewer, S.A., 2005. Fibroblast growth factor 15 functions as an enterohepatic signal to regulate bile acid homeostasis. Cell Metab. 2, 217–225.

Jang, J.H., Rickenbacher, A., Humar, B., Weber, A., Raptis, D.A., Lehmann, K., Stieger, B., Moritz, W., Soll, C., Georgiev, P., Fischer, D., Laczko, E., Graf, R., Clavien, P.A., 2012. Serotonin protects mouse liver from cholestatic injury by decreasing bile salt pool after bile duct ligation. Hepatology 56, 209–218.

Kubitz, R., Droge, C., Kluge, S., Stross, C., Walter, N., Keitel, V., Haussinger, D., Stindt, J., 2015. Autoimmune BSEP disease: disease recurrence after liver transplantation for progressive familial intrahepatic cholestasis. Clin. Rev. Allergy Immunol. 48, 273–284.

Li, F., Patterson, A.D., Krausz, K.W., Tanaka, N., Gonzalez, F.J., 2012. Metabolomics reveals an essential role for peroxisome proliferator-activated receptor alpha in bile acid homeostasis. J. Lipid Res. 53, 1625–1635.

Li, T., Jahan, A., Chiang, J.Y., 2006. Bile acids and cytokines inhibit the human cholesterol 7 alpha-hydroxylase gene via the JNK/c-jun pathway in human liver cells. Hepatology 43, 1202–1210.

Liu, A., Krausz, K.W., Fang, Z.Z., Brocker, C., Qu, A., Gonzalez, F.J., 2014a. Gemfibrozil disrupts lysophosphatidylcholine and bile acid homeostasis via PPARalpha and its relevance to hepatotoxicity. Arch. Toxicol. 88, 983–996.

Liu, A., Tanaka, N., Sun, L., Guo, B., Kim, J.H., Krausz, K.W., Fang, Z., Jiang, C., Yang, J., Gonzalez, F.J., 2014b. Saikosaponin d protects against acetaminophen-induced hepatotoxicity by inhibiting NF-kappaB and STAT3 signaling. Chem. Biol. Interact. 223, 80–86.

Liu, H., Liu, Y., Wang, L., Xu, D., Lin, B., Zhong, R., Gong, S., Podda, M., Invernizzi, P., 2010. Prevalence of primary biliary cirrhosis in adults referring hospital for annual health check-up in Southern China. BMC Gastroenterol. 10, 100.

Luo, M., Tan, Z., Dai, M., Song, D., Lin, J., Xie, M., Yang, J., Sun, L., Wei, D., Zhao, J., Gonzalez, F.J., Liu, A., 2017. Dual action of peroxisome proliferator-activated receptor alpha in perfluorodecanoic acid-induced hepatotoxicity. Arch. Toxicol. 91, 897–907.

Marhenke, S., Buitrago-Molina, L.E., Endig, J., Orlik, J., Schweitzer, N., Klett, S., Longerich, T., Geffers, R., Sanchez Munoz, A., Dorrell, C., Katz, S.F., Lechel, A., Weng, H., Krech, T., Lehmann, U., Dooley, S., Rudolph, K.L., Manns, M.P., Vogel, A., 2014. p21 promotes sustained liver regeneration and hepatocarcinogenesis in chronic cholestatic liver injury. Gut 63, 1501–1512.

Modica, S., Petruzzelli, M., Bellafante, E., Murzilli, S., Salvatore, L., Celli, N., Di Tullio, G., Palasciano, G., Moustafa, T., Halilbasic, E., Trauner, M., Moschetta, A., 2012. Selective activation of nuclear bile acid receptor FXR in the intestine protects mice against cholestasis. Gastroenterology 142 355–365.e351–354.

Molodecky, N.A., Kareemi, H., Parab, R., Barkema, H.W., Quan, H., Myers, R.P., Kaplan, G.G., 2011. Incidence of primary sclerosing cholangitis: a systematic review and meta-analysis. Hepatology 53, 1590–1599.

Nguyen, K.D., Sundaram, V., Ayoub, W.S., 2014. Atypical causes of cholestasis. World J. Gastroenterol. 20, 9418–9426.

Ofliver, E.A.F., 2009. EASL Clinical Practice Guidelines: management of cholestatic liver diseases. J. Hepatol. 51, 237–267.

Post, S.M., Duez, H., Gervois, P.P., Staels, B., Kuipers, F., Princen, H.M., 2001. Fibrates suppress bile acid synthesis via peroxisome proliferator-activated receptor-alpha-

mediated downregulation of cholesterol 7alpha-hydroxylase and sterol 27-hydroxylase expression. Arterioscler. Thromb. Vasc. Biol. 21, 1840–1845.

Sinal, C.J., Tohkin, M., Miyata, M., Ward, J.M., Lambert, G., Gonzalez, F.J., 2000. Targeted disruption of the nuclear receptor FXR/BAR impairs bile acid and lipid homeostasis. Cell 102, 731–744.

Sood, S., Gow, P.J., Christie, J.M., Angus, P.W., 2004. Epidemiology of primary biliary cirrhosis in Victoria, Australia: high prevalence in migrant populations. Gastroenterology 127, 470–475.

Stephanie, M., Irie, R., Sasaki, K., Hirata, Y., Narumoto, S., Fukuda, A., Sakamoto, S., Arai, K., Yoshioka, T., Kasahara, M., 2018. Histological changes of the intestinal mucosa in complications following a living donor liver transplantation for progressive familial intrahepatic cholestasis type 1. Pathol. Int.

Tan, Z., Liu, A., Luo, M., Yin, X., Song, D., Dai, M., Li, P., Chu, Z., Zou, Z., Ma, M., Guo, B., Chen, B., 2016. Geniposide Inhibits Alpha-Naphthylisothiocyanate-Induced Intrahepatic Cholestasis: The Downregulation of STAT3 and NF[Formula: see text]B Signaling Plays an Important Role. Am. J. Chin. Med. 44, 721–736.

Tanaka, Y., Aleksunes, L.M., Cui, Y.J., Klaassen, C.D., 2009. ANIT-induced intrahepatic cholestasis alters hepatobiliary transporter expression via Nrf2-dependent and independent signaling. Toxicol. Sci. 108, 247–257.

Tjandra, K., Sharkey, K.A., Swain, M.G., 2000. Progressive development of a Th1-type hepatic cytokine profile in rats with experimental cholangitis. Hepatology (Baltimore, Md.) 31, 280–290.

Wang, T., Zhou, Z.X., Sun, L.X., Li, X., Xu, Z.M., Chen, M., Zhao, G.L., Jiang, Z.Z., Zhang, L.Y., 2014. Resveratrol effectively attenuates alpha-naphthyl-isothiocyanate-induced acute cholestasis and liver injury through choleretic and anti-inflammatory mechanisms. Acta Pharmacol. Sin. 35, 1527–1536.

Yuan, Y., Xi, Y., Chen, J., Zhu, P., Kang, J., Zou, Z., Wang, F., Bu, S., 2017. STAT3 stimulates adipogenic stem cell proliferation and cooperates with HMGA2 during the early stage of differentiation to promote adipogenesis. Biochem. Biophys. Res. Commun. 482, 1360–1366.

Zhang, A., Jia, Y., Xu, Q., Wang, C., Liu, Q., Meng, Q., Peng, J., Sun, H., Sun, P., Huo, X., Liu, K., 2016. Dioscin protects against ANIT-induced cholestasis via regulating Oatps, Mrp2 and Bsep expression in rats. Toxicol. Appl. Pharmacol. 305, 127–135.

Zhang, X., Ma, Z., Liang, Q., Tang, X., Hu, D., Liu, C., Tan, H., Xiao, C., Zhang, B., Wang, Y., Gao, Y., 2015. Tanshinone IIA exerts protective effects in a LCA-induced cholestatic liver model associated with participation of pregnane X receptor. J. Ethnopharmacol. 164, 357–367.

Zhou, X., Cao, L., Jiang, C., Xie, Y., Cheng, X., Krausz, K.W., Qi, Y., Sun, L., Shah, Y.M., Gonzalez, F.J., Wang, G., Hao, H., 2014. PPARalpha-UGT axis activation represses intestinal FXR-FGF15 feedback signalling and exacerbates experimental colitis. Nat. Commun. 5, 4573.